INTERNATIONAL JOURNAL OF CLIMATOLOGY
Int. J. Climatol. **38**: 1353–1365 (2018)
Published online 29 August 2017 in Wiley Online Library
(wileyonlinelibrary.com) DOI: 10.1002/joc.5250

Impact of the boreal summer quasi-biweekly oscillation on Eastern North Pacific tropical cyclone activity

Haikun Zhao,[a]* Graciela B. Raga[b] and Philip J. Klotzbach[c]

[a] *Key Laboratory of Meteorological Disaster of the Ministry of Education, Joint International Research Laboratory of Climate and Environment Change, Collaborative Innovation Center on Forecast and Evaluation of Meteorological Disasters, Pacific Typhoon Research Center, Earth System Modelling Center, Nanjing University of Information Science and Technology, China*

[b] *Centro de Ciencias de la Atmósfera, Universidad Nacional Autónoma de México, Mexico City, Mexico*

[c] *Department of Atmospheric Science, Colorado State University, Fort Collins, CO, USA*

ABSTRACT: Several studies have focused on the impact of the Madden–Julian Oscillation (MJO, with a period between 30 and 60 days) on boreal summer tropical cyclone (TC) activity over the Eastern North Pacific (ENP) basin. The quasi-biweekly oscillation (QBWO), with a period of about 20 days, is another dominant mode of intra-seasonal variability during the boreal summer over the ENP basin. There have been fewer studies focused on the influence of the QBWO on tropical cyclogenesis over the ENP basin. The exploratory analyses performed in this study suggest that the QBWO has a strong impact on boreal summer ENP TC activity, with enhanced TC activity during the convectively active phase.

The significant increase (decrease) of tropical cyclogenesis events during the convectively active (inactive) QBWO phase is found to be closely associated with the strengthening (weakening) of the low-level cyclonic circulation and increasing (decreasing) mid-level relative humidity (vertical wind shear) over the ENP. Mid-level relative humidity and low-level vorticity are found to be the two most important players in modulating TC genesis location and frequency, based upon the analyses of the anomalous genesis potential index pattern and its magnitude associated with the QBWO. Associated with changes in TC location and large-scale steering flows, distinct difference in TC tracks during different QBWO phases can be readily found and thus cause substantial differences in basin-wide TC intensity. This study enhances our understanding of the modulation of intra-seasonal oscillations on boreal summer ENP TC activity and has the potential to aid in the sub-seasonal prediction of ENP TC activity.

KEY WORDS quasi-biweekly oscillation; tropical cyclone; genesis potential index; Eastern North Pacific

Received 17 April 2017; Revised 25 June 2017; Accepted 26 July 2017

1. Introduction

The Eastern North Pacific (ENP) basin is the second most active tropical cyclogenesis region in the world, experiencing an average of 14 named tropical cyclones (TCs) per year (Chu, 2004). These TCs can cause large financial damage to Mexico and, on occasion, to the southwestern United States (Pielke and Landsea, 1998; Pielke *et al.*, 2008; Emanuel, 2011). A better understanding of ENP TC activity on various time scales and the associated physical causes, therefore, has profound socio-economic impact and intense scientific interest.

On the intra-seasonal time scale, the Madden–Julian Oscillation (MJO, Madden and Julian, 1971, 1972), a well-known dominant intra-seasonal oscillation (ISO) mode, can significantly modulate ENP TC activity. There are generally more TCs observed over the ENP basin during the convectively active phase and fewer TCs observed during the suppressed convective phase (Molinari *et al.*, 1997; Maloney and Hartmann, 2000a, 2000b; Maloney and Dickinson, 2003; Aiyyer and Molinari, 2008; Camargo *et al.*, 2009; Barrett and Leslie, 2009). These studies suggested that the distinct differences during the different MJO phases are largely due to changes in environmental conditions or wave accumulation in terms of barotropic energy conversion. Camargo *et al.* (2009), based upon the genesis potential index (GPI) originally proposed by Emanuel and Nolan (2004), noted that mid-level relative humidity was the largest contributor to global TC genesis with a secondary contribution from the low-level vorticity. In contrast, vertical wind shear and potential intensity (PI) contributed only weakly to TC genesis. In order to capture the detailed features of ENP TC genesis, Jiang *et al.* (2012) investigated the actual TC genesis during different MJO phases over the ENP basin and re-examined the roles of the four GPI terms (i.e. mid-level relative humidity, low-level vorticity, vertical wind shear and PI) associated with the MJO in modulating ENP TC genesis. The results of Jiang *et al.* (2012) are consistent with those of Camargo *et al.* (2009), in that mid-level relative humidity and low-level vorticity

* Correspondence to: H. Zhao, Pacific Typhoon Research Center, Key Laboratory of Meteorological Disaster of Ministry of Education, Nanjing University of Information Science and Technology, Nanjing 210044, China. E-mail: zhk2004y@gmail.com

remained the two most important factors affecting ENP TC genesis frequency. Vertical wind shear may also play an important role in modulating TCs over certain area of the ENP basin during specific MJO phases (Camargo *et al.*, 2009; Jiang *et al.*, 2012).

Most existing studies on the intra-seasonal modulation of ENP TC activity focus on the modulation by the MJO. There is, however, another leading intra-season oscillation (ISO): the quasi-biweekly oscillation (referred to as the QBWO). Previous studies, by Jiang and Waliser (2008, 2009) and Serra *et al.* (2014), report that the QBWO exhibits a northwestward propagation, although the detailed physical mechanism of its origin remains unclear. Those studies also indicate that the large-scale circulations over the ENP basin undergo substantial changes during the different QBWO phases and, thus, should affect ENP TC activity. However, the impact of the boreal summer QBWO mode on ENP TC activity has been less investigated than the impact of the MJO on ENP TC activity.

This study follows an approach similar to previous studies (Camargo *et al.*, 2009; Jiang *et al.*, 2012; Zhao *et al.*, 2015a, 2015b), to systematically investigate the modulation of the QBWO on ENP TC genesis, TC tracks and TC intensity. The rest of this paper is arranged as follows: Section 2 describes the datasets used and the methodology implemented to identify the QBWO during the boreal summer for the period 1998–2015. The modulation of ENP TC activity by the QWBO including genesis, track and intensity is investigated in Section 3. Section 4 illustrates the modulation of large-scale factors affecting tropical cyclogenesis by the QBWO mode and further explores the relative role of large-scale factors affecting tropical cyclogenesis through analysis of the GPI. A summary and conclusions are presented in Section 5.

2. Data and methods

2.1. Data

TC data is obtained from the U.S. hurricane database (HURDAT2) best track dataset through the U.S. National Oceanic and Atmospheric Administration (NOAA)/National Hurricane Center (NHC) (Landsea and Franklin, 2013), which includes the position (in latitude and longitude) and intensity (in knots) of each TC at 6-hourly intervals (available from http://www.nhc.noaa.gov/data/#hurdat). Only TCs with an intensity greater than or equal to 34 knots from May to October during the period 1998–2015 are considered in this study. Accumulated Cyclone Energy (ACE) (Bell *et al.*, 2000) and the number of intense TCs with intensity equal to or greater than 96 knots (i.e. the number of Cat. 3–5 TCs) are estimated to further characterize TC activity.

Rainfall observations during 1998–2015 derived from the Tropical Rainfall Measuring Mission (TRMM) version 3B42 (Huffman *et al.*, 2007) are used to identify the boreal summer QBWO mode over the ENP basin. Such data processing has been widely used in previous studies (Jiang and Waliser, 2008, 2009; Jiang *et al.*, 2012; Zhao *et al.*, 2015a, 2015b, 2016; Neena *et al.*, 2017). The TRMM 3B42 rainfall is used to identify the QBWO mode over the ENP basin. It is a global precipitation product in a zonal belt from 50°S to 50°N based on multi-satellite and rain gauge analyses, with a 3-h temporal resolution and a 0.25° spatial resolution.

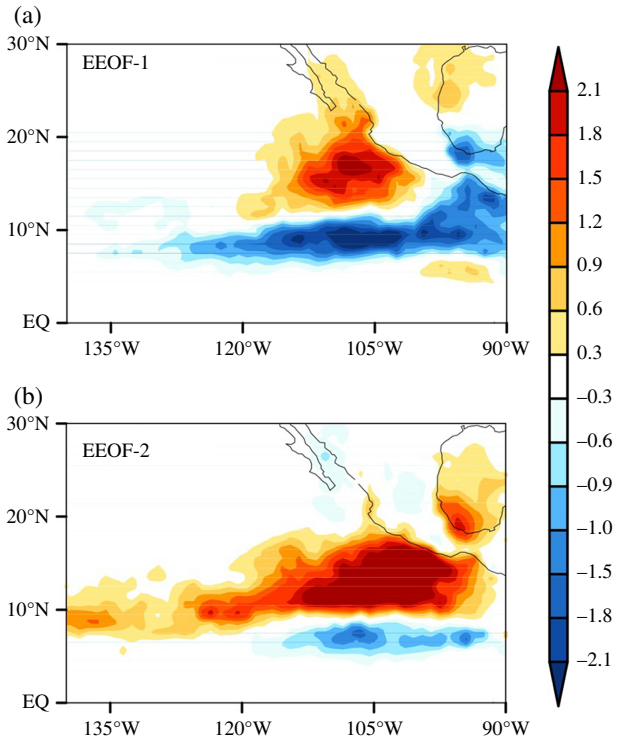

Figure 1. (a) EEOF-1 and (b) EEOF-2 PCs regressed onto the 10- to 30-day filtered rainfall anomalies from May to October for the period 1998–2015. [Colour figure can be viewed at wileyonlinelibrary.com].

Daily winds, relative humidity, temperature and sea-surface temperature (SST) are derived from the European Center for Medium-Range Weather Forecasts (ECMWF) Era-Interim reanalysis (Dee *et al.*, 2011) with a horizontal resolution of 1.5° × 1.5°. These large-scale fields are investigated in order to explore possible physical causes responsible for the impact of the QBWO mode on ENP TC activity during 1998–2015.

2.2. Identification of the QBWO mode over the ENP basin

Extended empirical orthogonal function (EEOF) analysis (Weare and Nasstrom, 1982) is used in this study to extract the ISO modes, following previous studies (Jiang and Waliser, 2008, 2009; Jiang *et al.*, 2012; Zhao *et al.*, 2015a, 2015b, 2016; Neena *et al.*, 2017). EEOF analysis of the daily 10- to 30-day band-pass filtered TRMM rainfall anomalies during the boreal summer for the period 1998–2015 is performed (as in Jiang *et al.* (2012) and Zhao *et al.* (2015a, 2015b)), with temporal lags of 9 days over the following domain: (0°–30°N, 140°–90°W). The boreal summer QBWO mode over the ENP basin is identified by the first leading pair of EEOF modes (Figure 1), as shown in Jiang and Waliser (2008, 2009). The first leading

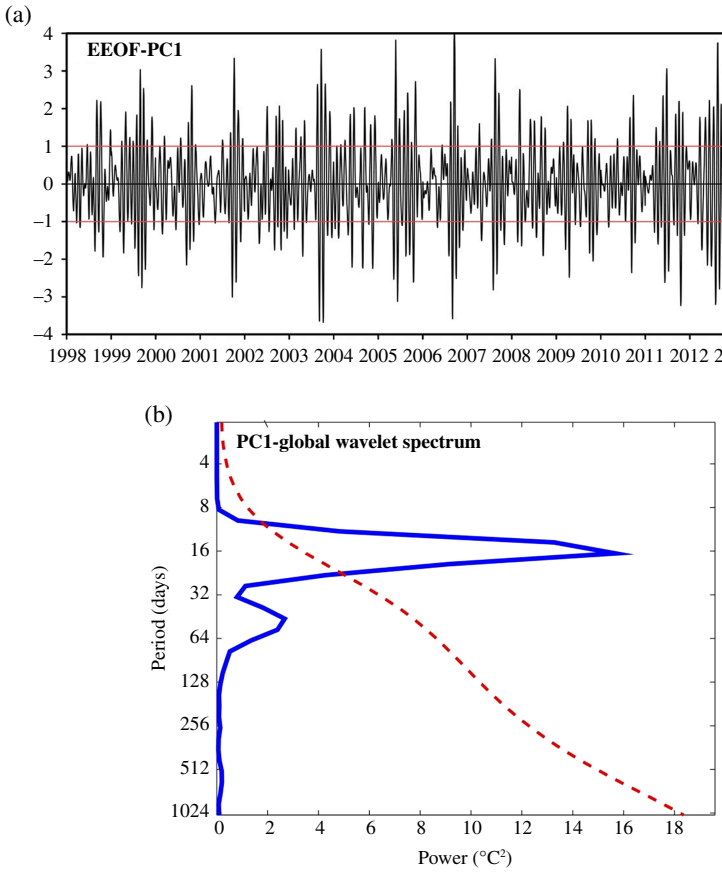

Figure 2. (a) Time series of PC1 for EEOF-1 mode from May to October for the period 1998–2015 and (b) the corresponding spectrum analyses of PC1. [Colour figure can be viewed at wileyonlinelibrary.com].

pair, EEOF1 and EEOF2, represents propagating features of the first leading mode of the 10–30-day band during the boreal summer for the period 1998–2015. Based on the formula proposed by North *et al.* (1982), we compute the variance explained by each EEOF mode and find that EEOF1 and EEOF2 stand out from the remaining EEOF modes. Moreover, these two EEOF modes are well separated from each other. The first two EEOFs contribute 5.9% of the total anomalous variances of 10- to 30-day band-pass filtered daily data with a lag of 9 days. The time series of the principal components (PCs) of EEOF1 and EEOF2 (hereafter PC1 and PC2, respectively) are illustrated in Figure 2. Further spectral analysis of PC1 suggests a dominant period of about 20 days, which is also found for PC2 (figure not shown). These features are generally consistent with previous studies (Jiang and Waliser, 2008, 2009; Jiang *et al.*, 2011; Serra *et al.*, 2014). Overall, the first leading EEOF mode (i.e. EEOF1 and EEOF2 modes) of the observed daily rainfall anomalies captures well the QBWO mode. An obvious northwestward propagation for the QBWO during the boreal summer over the ENP basin is seen from the evolution of EEOF-1 mode (EEOF-2 mode) from lag − 9 to lag + 9 (Figure 3). These results increase our confidence in adopting the EEOF method to extract the boreal summer QBWO mode over the ENP basin.

The QBWO phases are defined following the work of Wheeler and Hendon (2004), in which the first two leading PCs are used to determine daily QBWO amplitudes and phases, ranging from phases 1 to 8. Once the eight phases are obtained, each available day is assigned into one of these eight phases. Composite maps of observed rainfall are obtained by averaging the 10- to 30-day band-pass filtered rainfall anomalies over each QBWO phase, based on selected strong QBWO events during the boreal summer for the period 1998–2015. A strong QBWO event is defined as $\sqrt{PC1^2 + PC2^2} \geq 1.0$. The TC data are then binned into one of these eight phases, e.g. each TC is assigned to a specific phase of the QBWO mode based on the day of TC formation. The number of Cat. 3–5 TCs is classified based on the QBWO phase on the day that the TC first reached Cat. 3–5 hurricane strength. The total ACE for a specific QBWO phase is computed as the sum of the ACE for the total QBWO days during a specific QBWO phase. The total Cat. 3–5 TCs and ACE for different QBWO phases is divided by the respective QBWO days to obtain the daily Cat. 3–5 TCs and ACE.

2.3. Assessing the role of environmental factors

To assess the relative role of the large-scale controls of ENP tropical cyclogenesis, the GPI is used as a diagnostic

tool in this study. Emanuel and Nolan (2004) developed GPI with the following Equation 1:

$$GPI = \underbrace{\left|10^5\xi\right|^{3/2}}_{\eta}\underbrace{\left(\frac{H}{50}\right)^3}_{\gamma}\underbrace{\left(\frac{V_{\text{pot}}}{70}\right)^3}_{\phi}\underbrace{\left(1+0.1\times V_{\text{shear}}\right)^{-2}}_{S} \tag{1}$$

where ξ is the 850 hPa absolute vorticity (s^{-1}), H is the 600 hPa relative humidity (%), V_{pot} is the PI ($m\,s^{-1}$), providing an upper bound on TC intensity of a TC under given specific environmental thermodynamic conditions (Bister and Emanuel, 2002), and V_{shear} is the vertical wind shear, computed as the magnitude of the vector difference between winds at 850 and 200 hPa ($m\,s^{-1}$). The GPI can be represented by these four components: which is expressed by the four terms η, γ, ϕ, and S, which, respectively correspond to 850 hPa absolute vorticity, 600 hPa relative humidity, PI and vertical wind shear. Studies have suggested that GPI can capture well both inter-annual variations of TC genesis in several basins (Camargo *et al.*, 2007) as well as intra-seasonal variability (Camargo *et al.*, 2009; Jiang *et al.*, 2012; Zhao *et al.*, 2015a, 2015b). Similar to these previous studies on the intra-seasonal time scale, each of these four linear terms contributing to GPI anomalies can be decomposed into two components: a climatological annual component and a departure, which contains variability on various time scales from synoptic to inter-annual. The GPI anomalies associated with the QBWO can be written as the sum of 15 terms, and following Camargo *et al*. (2009), the GPI anomalies associated with the QBWO can be decomposed into four linear terms. Their relative roles can be further explored by specifying one term with the corresponding anomaly while the other three terms are specified with their summer mean climatological values. Moreover, the sum of the total remaining 11 terms including high-order variances of two or more terms of the four variables is used to evaluate the contributions of nonlinear terms. Specifically, any environmental variable can be partitioned into a climatological annual cycle component (X) and a fluctuation (X'), which contains variability on synoptic, intra-seasonal, and inter-annual time scales (i.e. $X = \overline{X} + X'$) where X represents each GPI component in Equation 1: η, γ, ϕ and S. Then the anomalous GPI associated with the QBWO (GPI^{QBWO}) can be expressed in terms of the four GPI components as follows:

$$\begin{aligned}\text{GPI}^{\text{QBWO}} &= \overline{\gamma}.\overline{\phi}.\overline{s}.\eta^{\text{QBWO}} + \overline{\eta}.\overline{\phi}.\overline{s}.\gamma^{\text{QBWO}} + \overline{\eta}.\overline{\gamma}.\overline{s}.\phi^{\text{QBWO}} + \overline{\eta}.\overline{\gamma}.\overline{\phi}.s^{\text{QBWO}} \\ &+ \left\{\begin{array}{l}\overline{\gamma}.\overline{\phi}.\left(s'.\eta'\right)^{\text{QBWO}} + \overline{\gamma}.\overline{s}.\left(\phi'.\eta'\right)^{\text{QBWO}} + \overline{\gamma}.\overline{\eta}.\left(\phi'.s'\right)^{\text{QBWO}} + \overline{\phi}.\overline{s}.\left(\gamma'.\eta'\right)^{\text{QBWO}} + \overline{\phi}.\overline{\eta}.\left(\gamma'.s'\right)^{\text{QBWO}} + \overline{s}.\overline{\eta}.\left(\gamma'.\phi'\right)^{\text{QBWO}} \\ +\overline{\gamma}.\left(\phi'.s'.\eta'\right)^{\text{QBWO}} + \overline{\phi}.\left(\gamma'.s'.\eta'\right)^{\text{QBWO}} + \overline{s}.\left(\eta'.\gamma'.\phi'\right)^{\text{QBWO}} + \overline{\eta}.\left(\gamma'.\phi'.s'\right)^{\text{QBWO}} \\ +\left(\gamma'.\phi'.s'.\eta'\right)^{\text{QBWO}}\end{array}\right\}\end{aligned} \tag{2}$$

The total GPI anomalies associated with the QBWO can be decomposed into the sum of the role of the nonlinear term and the four linear terms, which are associated with the QBWO of each of the four factors while the other three terms remain constant at their summer climatological values (i.e. the first four terms in Equation 2). Moreover, the contributions of the nonlinear term are examined by the terms that include high-order variances of two or more of the four factors (a total of 11 terms included within the brackets in Equation 2).

2.4. Quantification of TC activity

The daily genesis rate (DGR), which is defined as the number of TC genesis events divided by the number of days for a particular QBWO phase, is used to quantify TC frequency. A statistical test was performed assuming TC frequency is uniform among QBWO phases as the null hypothesis, following previous studies (Hall *et al.*, 2001; Kim *et al.*, 2008; Klotzbach, 2010; Li and Zhou, 2013). A statistical parameter Z is defined as:

$$Z = \frac{P - P_e}{\sqrt{P_e\left(1-P_e\right)/N}}$$

where P_e represents the climatological value of DGR, while P is the DGR, and N is the number of days of a particular QBWO phase. With this definition, the parameter Z follows a Gaussian distribution, and the critical values for the test are $Z = \pm 1.65(\pm 1.96)$ for the 90% (95%) confidence level, respectively.

3. Impact of the QBWO on ENP TC activity

Figure 4 shows the standard deviation of 10- to 30-day (Figure 4(a)) and 30- to 60-day (Figure 4(b)) band-pass filtered rainfall anomalies along with TC genesis events during May–October for the period 1998–2015 in the ENP basin. Most TCs coincide with vigorous intra-seasonal activity in the 10- to 30-day band and 30- to 60-day band (Figure 4). Additionally, stronger variance is found for the 10- to 30-day band than for the 30- to 60-day band over the ENP basin. Similar results are also found over the WNP basin (Li and Zhou, 1995). These findings are suggestive of a possible QBWO modulation on ENP TC activity.

It is readily seen in Figure 5 and Table 1 that the QBWO has a strong modulation on TC genesis frequency over the ENP basin in terms of both TC counts (Figure 5(a)) and DGR (Figure 5(b)). Fewer TC genesis events occur during phases 1, 2, 3 and 8 with a significant decrease from the climatological average during phases 1–3 (95% level), while more TC genesis events occur during phases 4, 5, 6 and 7 with a significant increase during phases 4 and 6 (90% level) and 5 (95% level). Reduced TCs observed during phases 1, 2, 3 and 8 are associated with negative rainfall anomalies, while increased TCs during phases 4, 5, 6 and 7 correspond to positive rainfall anomalies

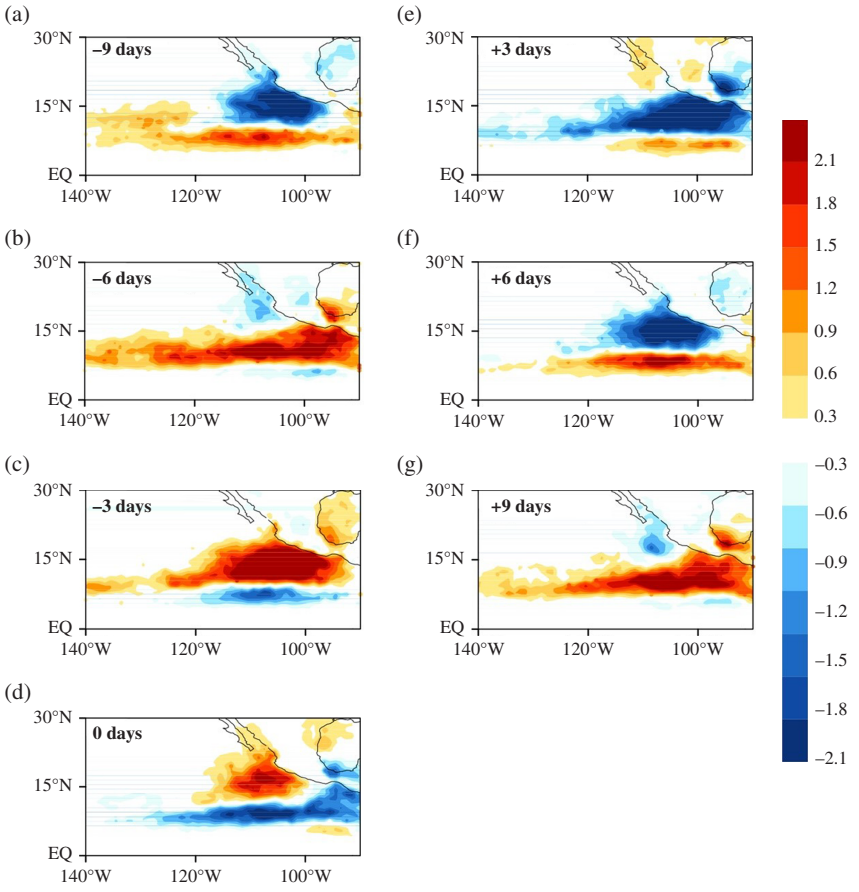

Figure 3. Lead-lagged regression patterns of TRMM rainfall *versus* the time series of EEOF-1 PCs from lag −9 days to lead +9 days during May–October for the period 1998–2015: (a) −9 days, (b) −6 days, (c) −3 days, (d) 0 days, (e) +3 days, (f) +6 days and (g) +9 days. [Colour figure can be viewed at wileyonlinelibrary.com].

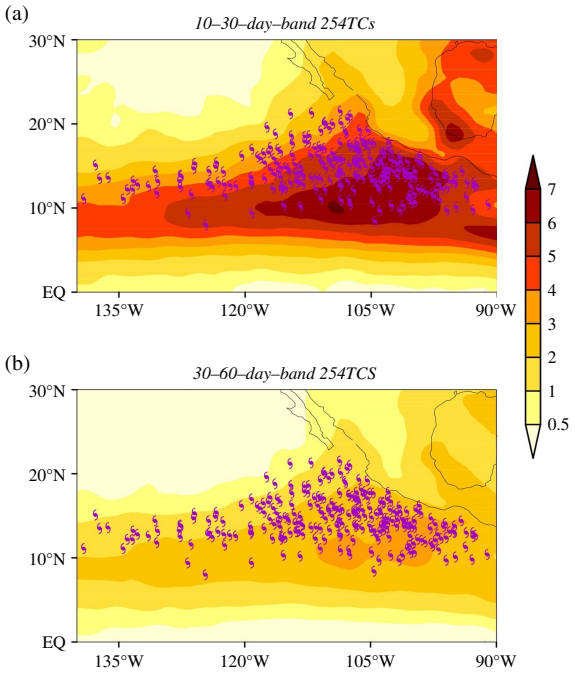

Figure 4. Standard deviation of the (a) 10- to 30-day and (b) 30- to 60-day band-pass filtered rainfall anomalies from May to October for the period 1998–2015. [Colour figure can be viewed at wileyonlinelibrary.com].

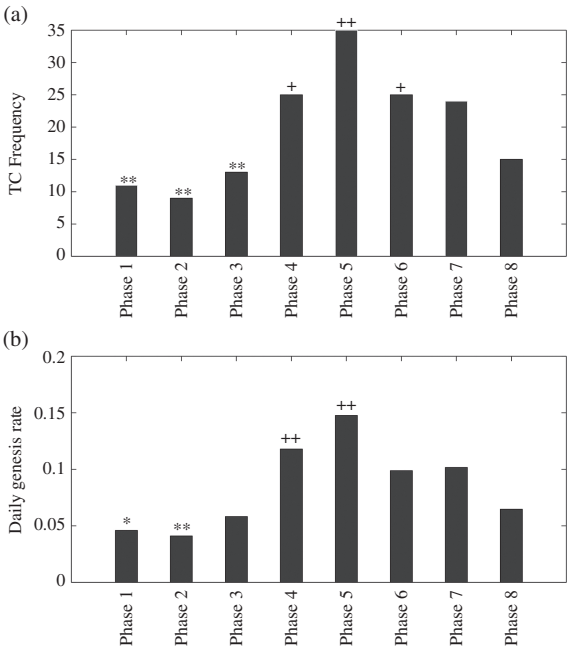

Figure 5. (a) TC counts and (b) DGR of TCs for all QBWO phases from May to October for the period 1998–2015. The symbols "**" and "*" ("++" and "+") indicate the DGR is statistically significant from the eight-phase average at the 95 and 90% confidence level, respectively.

Table 1. Statistics of TC genesis latitude and longitude, number of TCs, number of cat. 3–5 TCs and ACE for different QBWO phases.[a]

	TC genesis latitude (°N)	TC genesis longitude (°E)	Number of TCs	Number of cat. 3–5 TCs	ACE (*1.0e+05 knot^2)
Total basin/Eastern ENP/Western ENP					
Phase 1	15.3+/15.6++/13.9	251.5/254.6/237.6**	11**/9**/2**	3/2/1	9.5*/7.8/1.7**
Phase 2	13.5**/14.2**/13.0**	246.2**/258.8++/236.2	9**/4**/5	3/0**/3++	11.5/1.9**/9.6++
Phase 3	15.1/14.5*/15.6++	248.0*/254.6/242.3	13**/6**/7	2**/1**/1	9.0**/4.6**/4.4
Phase 4	14.7/14.7/14.8	251.1/255.5/241.9+	25+/17++/8++	7+/6++/1	17.3++/14.0++/3.3
Phase 5	14.4/14.5*/13.7	254.9++/257.9++/242.8++	35++/28++/7	12++/10++/2++	25.9++/22.7++/3.2
Phase 6	14.2**/14.5*/13.5*	250.9/255.0/242.2	25+/18++/7	6/6++/0**	22.9++/18.7++/4.2
Phase 7	16.0++/15.4++/17.6++	251.2/254.8/242.6	24/17+/7	2**/2/0**	9.1**/8.3/0.8**
Phase 8	15.1/15.7++/13.8	249.1/253.8*/239.6	15/10*/5	3/2/1	8.2**/4.4**/3.8
Average of phases 1–8	14.8/14.9/14.5	250.4/255.6/240.4	19.63/13.63/6	4.75/3.63/1.13	14.2/10.3/3.9

[a]Phases of these variables are statistically enhanced (decreased) from the eight-phase average at 90 and 95% confidence are indicated by + and ++ (* and **), respectively.

(figure not shown). Lower DGR is also observed during phases 1, 2, 3 and 8, with a significant reduction occurring in phases 1 (90% level) and 2 (95% level). Higher DGR is observed during phases 4, 5, 6 and 7, with a significant increase at the 95% level occurring during phases 4 and 5. In addition, higher ACE is generally found during phases 4–7 and more Cat. 3–5 TCs during phases 4–6 (Table 1). In order to further highlight these observed differences, we combine phases 1, 2, 3 and 8 into one category named convectively inactive QBWO phase and phases 4, 5, 6 and 7 into another category named convectively active QBWO phase. The difference in DGR can be clearly seen in Figure 6. Significantly higher DGR (11.6%) at the 95% confidence level is seen during the active QBWO phase, compared to the climatological DGR value (7.7%). Significantly lower DGR is seen during the inactive QBWO phase (5.3%) at the 95% confidence level. This difference is associated spatially with the patterns of composite rainfall anomalies during convectively active and inactive QBWO phases (Figure 7). More TCs (109 TCs) are associated with positive rainfall anomalies during the convectively active QBWO phase (Figure 7(a)), and fewer TCs (48 TCs) are associated with negative rainfall anomalies during the convectively inactive QBWO phase (Figure 7(b)).

In addition to the modulation by the QBWO of tropical cyclogenesis events and the DGR, TC genesis locations (Figures 8(a) and (b); Table 1) show a difference with a moderate eastward and southward shift in TC genesis during the convectively active phase compared to that during the convectively inactive phase, as indicated by the contours of the probability density function. This suggests that during the convectively active phase TCs are more likely to form closer to the Mexican coast. Such

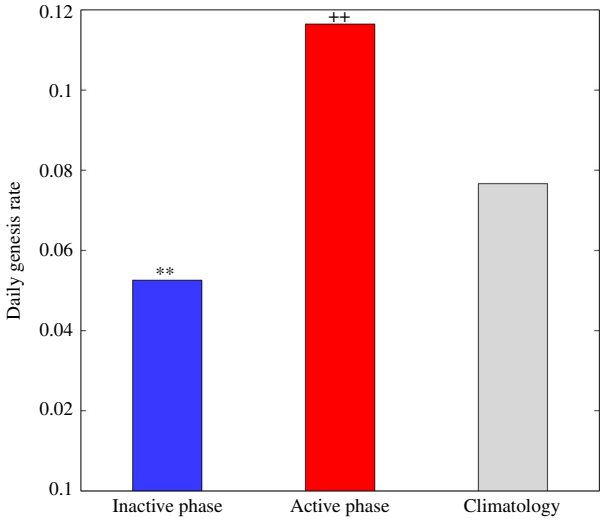

Figure 6. DGR of TCs for the inactive and active QBWO phases and climatology. The symbols "**" and "++" indicate that the DGR of TCs are statistically significant from the climatology at the 95% confidence level. [Colour figure can be viewed at wileyonlinelibrary.com].

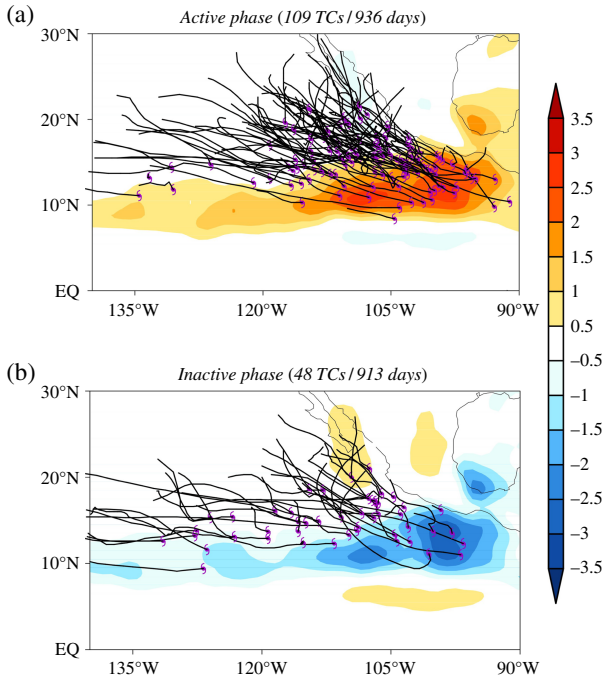

Figure 7. Composite rainfall anomalies (shading) for the: (a) active and (b) inactive QBWO phases from May to October for the period 1998–2015. Also plotted are TC tracks. [Colour figure can be viewed at wileyonlinelibrary.com].

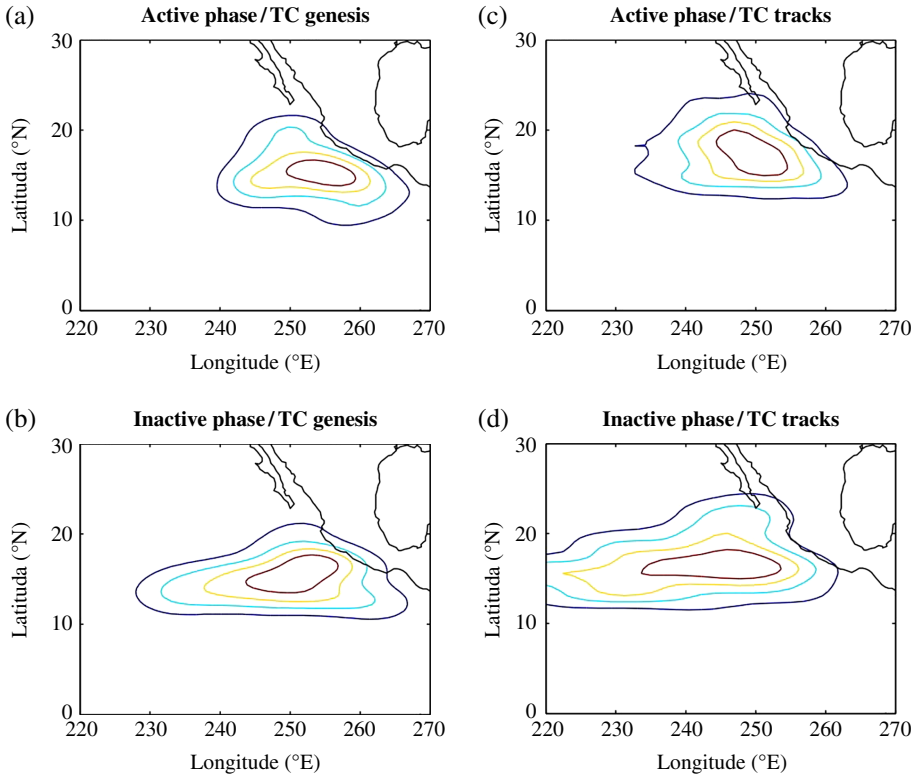

Figure 8. Contours of probability density function of occurrence of TC genesis for: (a) active and (b) inactive QBWO phases. Contours of the Probability Density Function of occurrence of TC tracks for (c) active and (d) inactive QBWO phases. [Colour figure can be viewed at wileyonlinelibrary.com].

a southward shift of TC genesis during the convectively active phase may partly contribute to the significant north–south variations of TC genesis locations over the ENP basin as suggested by Wang *et al.* (2016). The details of this issue deserve further study. Moreover, significant differences are also seen in TC tracks with more TCs having westward trajectories during the convectively inactive phase and more TCs having northwestward trajectories during the convectively active phase (Figures 8(c) and (d)). Such changes of trajectories are closely associated with the changes of the large-scale steering flow (Figure 9). The large-scale steering flow is computed as the wind averaged from 850 to 300 hPa, a definition adopted in previous studies (Wu and Wang, 2004; Wu *et al.,* 2005; Zhao *et al.*, 2010; Wang *et al.*, 2011; Zhao *et al.*, 2014). Figures 9(a) and (b) show the composite large-scale steering flow for the convectively active and inactive phases, as well as the difference in the large-scale steering flow between the active and inactive phases (Figure 9(c)). Note the cyclonic circulation anomaly seen over the main development region (Figure 9(c)), consistent with increased TCs during the convectively active phase. Meanwhile, an obvious westerly anomaly is seen north of 20°N, which favours more northwestward tracks.

The QBWO not only modulates TC genesis location and trajectories, it is also associated with significant differences in intensity (Figure 10). There is higher ACE during the convectively active phase than during the convectively inactive phase (Figure 10(a)). Closer examination suggests that the significant difference of ACE between the convectively active and inactive phases is mainly due to the significant difference of TC number especially for intense TCs. More major hurricanes (Categories 3 through 5; Cat. 3–5 TCs) are observed during the convectively active phase than during the convectively inactive phase (Figure 10(b)). To better quantify the impact of the QBWO on basin-wide TC intensity, total ACE and the number of major hurricanes for different phases is divided by the respective QBWO days to obtain the daily ACE and DGR for major hurricanes (Figures 10(c) and (d)). Compared to climatology, significantly higher ACE and DGR of major hurricanes is seen (at a 95% confidence level) during the convectively active phase. Conversely, significantly lower ACE and DGR of major hurricanes is seen during the convectively inactive phase.

4. Importance of large-scale factors affecting TC genesis

Figure 11 displays composite anomalies of 850 hPa winds and 850 hPa relative vorticity, while Figure 12 shows 600 hPa relative humidity and vertical wind shear during the convectively active and inactive QBWO phases. More TCs generally occurred with cyclonic circulation anomalies at 850 hPa (Figure 11) and positive mid-level relative humidity anomalies (Figure 12; in shading) that are favoured during the convectively active phase. Conversely, fewer TCs generally occurred with anti-cyclonic

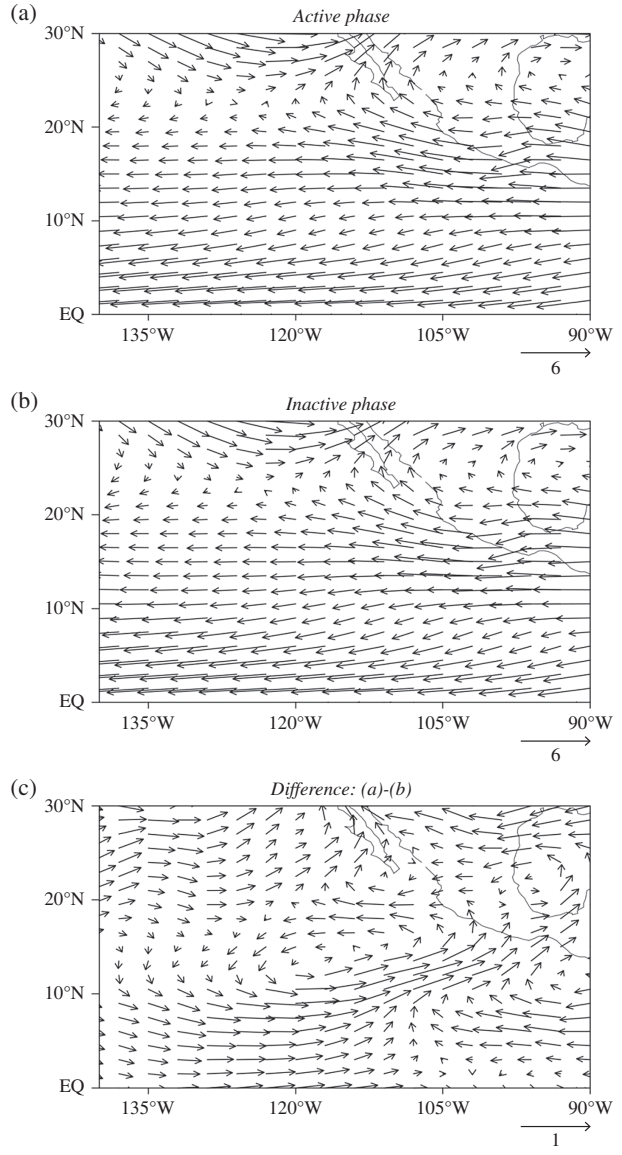

Figure 9. Large-scale steering flow averaged from 850 to 300 hPa for the: (a) active QBWO phase, (b) inactive QBWO phase and (c) the difference between (a) and (b).

circulation anomalies at 850 hPa (Figure 11) and negative mid-level relative humidity anomalies (Figure 12; in shading) that are favoured during the convectively inactive phase. More TCs are observed in regions of negative vertical wind shear anomalies, and fewer TCs are associated with positive vertical wind shear anomalies (Figure 12; contour). As suggested in previous studies (Gray, 1968; McBride and Zehr, 1981), these large-scale parameters are more favourable for tropical cyclogenesis events, and thus TCs are clearly seen here to be enhanced during the convectively active QBWO phase.

In order to explore the key factors associated with the QBWO's modulations of ENP basin TC genesis, the relative role of large-scale factors is further assessed by utilizing a GPI analysis following the approach in Jiang *et al.* (2012) and Zhao *et al.* (2015a, 2015b) and described briefly in Section 2.3. Figures 13(a) and (b) show the evolution of GPI anomalies along with TC genesis during the convectively active and inactive QBWO phases. Corresponding to the observed rainfall anomalies displayed in Figure 7, positive (negative) GPI anomalies are generally associated with active (inactive) convective phases. The majority of TCs occur over regions with positive GPI anomalies. Note that a small number of TCs can also be found over regions with negative GPI anomalies, which may be attributed to other factors not considered in the definition of GPI (Equation 1) or not associated with the QBWO mode. Nevertheless, the GPI anomalies have considerable skill in capturing TC genesis over the ENP basin associated with the QBWO. Therefore, we proceed to isolate the role of each of the factors included in the GPI in contributing to the TC genesis associated with the QBWO.

The spatial distribution of each of the factors of the GPI anomalies associated with the convectively active QBWO phases is seen in Figures 13(c) and (e), and 14(a), (c) and (e), respectively. Positive GPI anomalies varying each of the four environmental factors are highly spatially correlated with the TC genesis events during the convectively active phase. If the ENP is divided into eastern and western sub-regions at 112°W, as suggested by Ralph and Gough (2009) and Jien *et al.* (2015), it is clear that TC genesis is not spatially uniform. TC genesis events are consistent with the distribution of GPI anomalies by varying each of the four factors over the two sub-regions, with somewhat lower consistency with GPI anomalies while varying PI over the western sub-region. These findings suggest that all four factors play a positive role in contributing to the GPI anomalies associated with the QBWO. In contrast, the spatial distribution of each of the factors of the GPI anomalies associated with inactive QBWO phases is displayed in Figures 13(d) and (f), and 14(b), (d) and (f). The GPI anomalies varying each of the four environmental factors during the inactive phase are not as consistent as during the active phase. In particular, the GPI anomalies varying vertical wind shear and PI do not align well with TC genesis events. The relative importance of each of the four environmental factors (as well as the nonlinear terms) will be assessed from the pattern correlation for the ENP basin and each of the two sub-regions and changes in magnitude of GPI anomalies.

As shown in Figure 15(a), these pattern correlation coefficients are significant at the 95% confidence level during the convectively active phase. In an operational setting, a pattern correlation of 0.60 is deemed as a lower limit for a field forecast that is synoptically useful (Wilks, 2006). This value has been used as the reference value to examine the performance of a model (Cheng and Chan, 2012) and to assess the importance of factors for the associated specific pattern (Zhao *et al.*, 2014). Over the whole ENP basin, low-level relative vorticity and mid-level relative humidity are the two most important contributors to the pattern of GPI anomalies during the active phase. These results are consistent with previous studies on other time scales (Camargo *et al.*, 2009; Jiang *et al.*, 2012; Zhao *et al.*, 2015a, 2015b). Note that the nonlinear term is

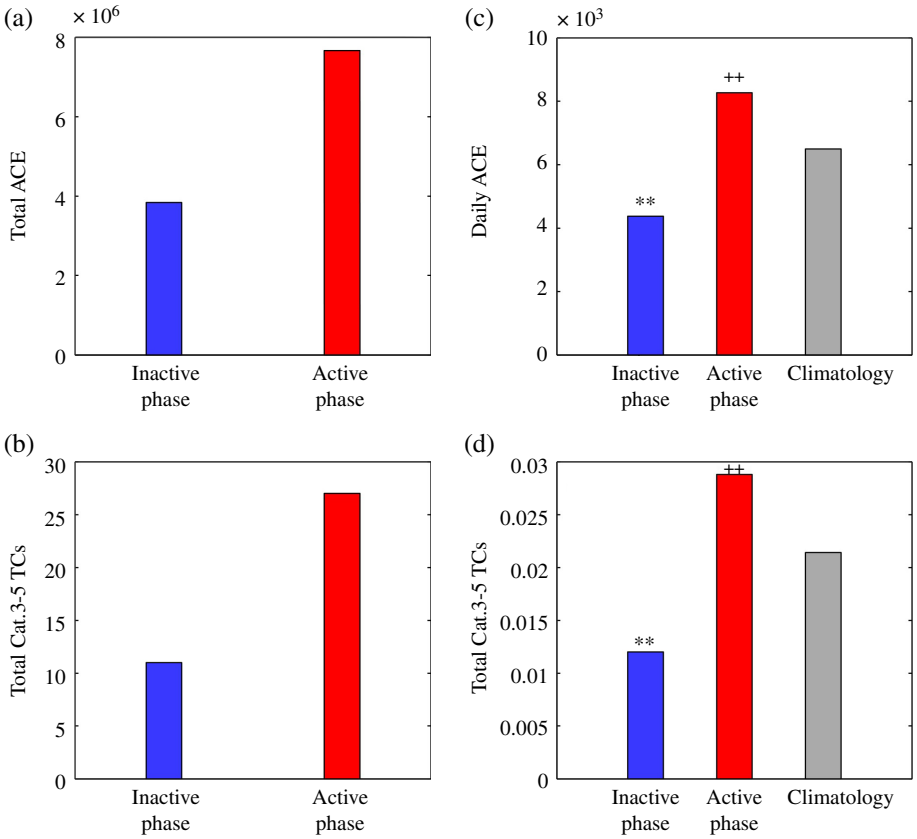

Figure 10. (a) ACE and (b) number of category 3–5 TCs for active and inactive QBWO phases. (c) Same as (a) but for daily ACE. (d) Same as (b) but for the DGR of Cat. 3–5 TCs. The symbols "**" and "++" indicate that the daily cat. 3–5 TCs and ACE are statistically significant from the climatology at the 95% confidence level. [Colour figure can be viewed at wileyonlinelibrary.com].

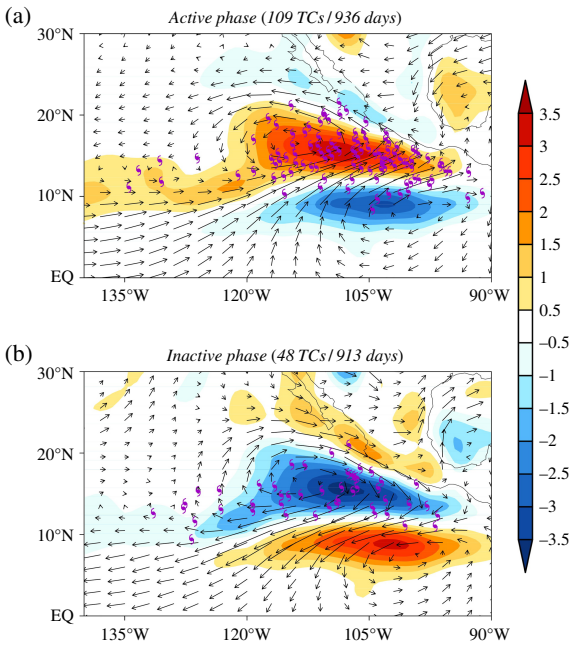

Figure 11. Composite 850 hPa wind anomalies (vectors) and relative vorticity anomalies (shading) from May to October for the period 1999–2015 for: (a) active and (b) inactive QBWO phases. The symbols indicate the location of TC genesis. [Colour figure can be viewed at wileyonlinelibrary.com].

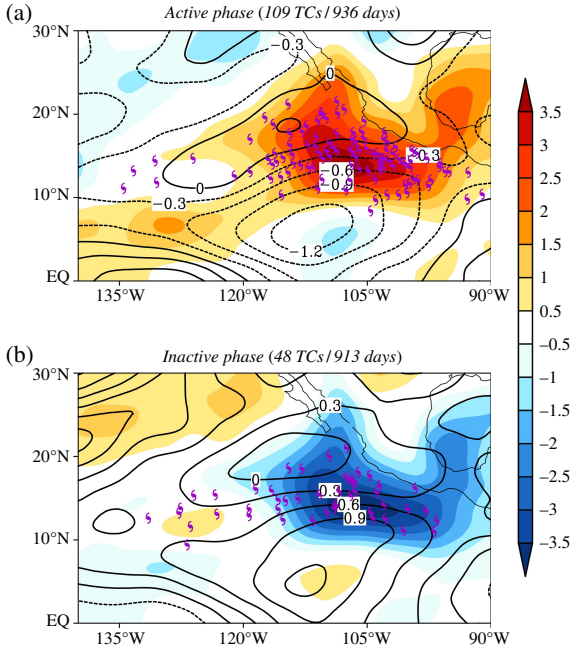

Figure 12. Composite 600 hPa relative humidity anomalies (shading) and vertical wind shear anomalies (contours) from May to October for the period 1998–2015, for: (a) active and (b) inactive QBWO phases. The symbols indicate the location of TC genesis. [Colour figure can be viewed at wileyonlinelibrary.com].

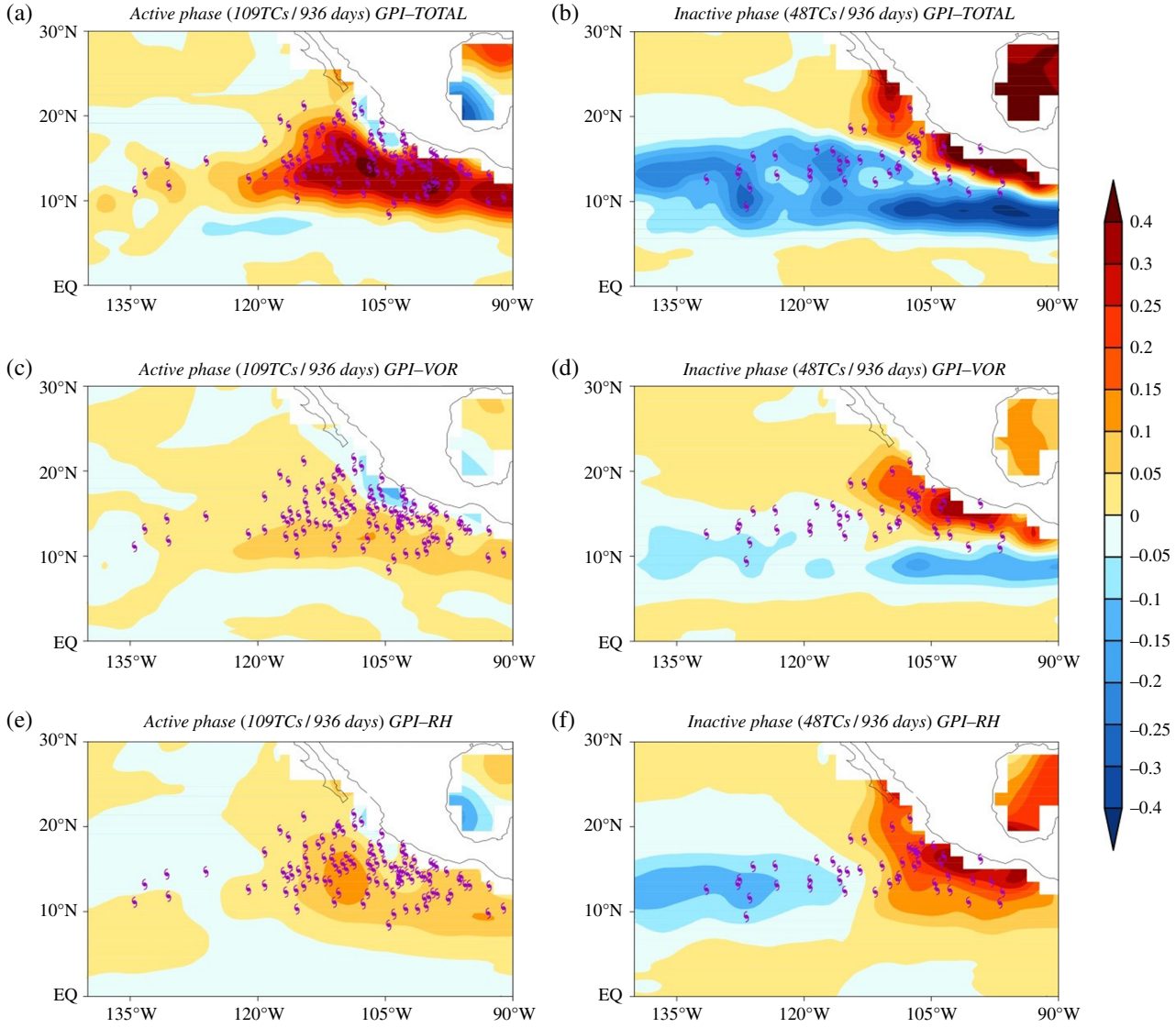

Figure 13. Composite GPI anomalies for (a) active and (b) inactive QBWO phases varying all four variables (GPI-TOTAL). (c) and (d) are the same as (a) and (b) but varying 850 relative vorticity (GPI-VOR). (e) and (f) are the same as (a) and (b) but varying 600 hPa relative humidity. [Colour figure can be viewed at wileyonlinelibrary.com].

also an important factor in contributing to the pattern of GPI anomalies, while the vertical wind shear and PI play a secondary role. Similar results are found for the two sub-regions, except for a relatively weak role of vertical wind shear over the eastern sub-region and a relatively weak role of PI over the western sub-region. During the convectively inactive phase, the pattern correlations also indicate that the low-level relative vorticity, mid-level relative humidity and nonlinear terms are the three most important contributors to the distribution of GPI anomalies over the total ENP basin, while the vertical wind shear and PI play a weak role (Figure 15(b)).

The contributions of the four environmental factors to the magnitude of GPI anomalies as a function of the QBWO phase are computed for the whole ENP basin as well as the two sub-regions and are displayed in Figure 16. The relative importance of each of the four terms of the GPI anomalies is largely dependent on the QBWO phase, consistent with previous studies (Jiang *et al.*, 2012; Zhao *et al.*, 2015a, 2015b). Mid-level relative humidity is the most important player in contributing to the GPI anomalies. The changes of GPI anomalies are due to the combined positive contributions from the four factors and the nonlinear term. During the convectively active phases, the four factors and the nonlinear term show consistent positive contributions. During the convectively inactive phase, the negative GPI anomalies are mainly from the low-level vorticity, vertical wind shear, PI and the nonlinear term. These negative GPI anomalies are partly cancelled by the positive contribution from 600 hPa relative humidity, especially over the eastern sub-region.

5. Summary

This study investigates the impact of the QBWO on the boreal summer ENP TC activity, a topic which has until

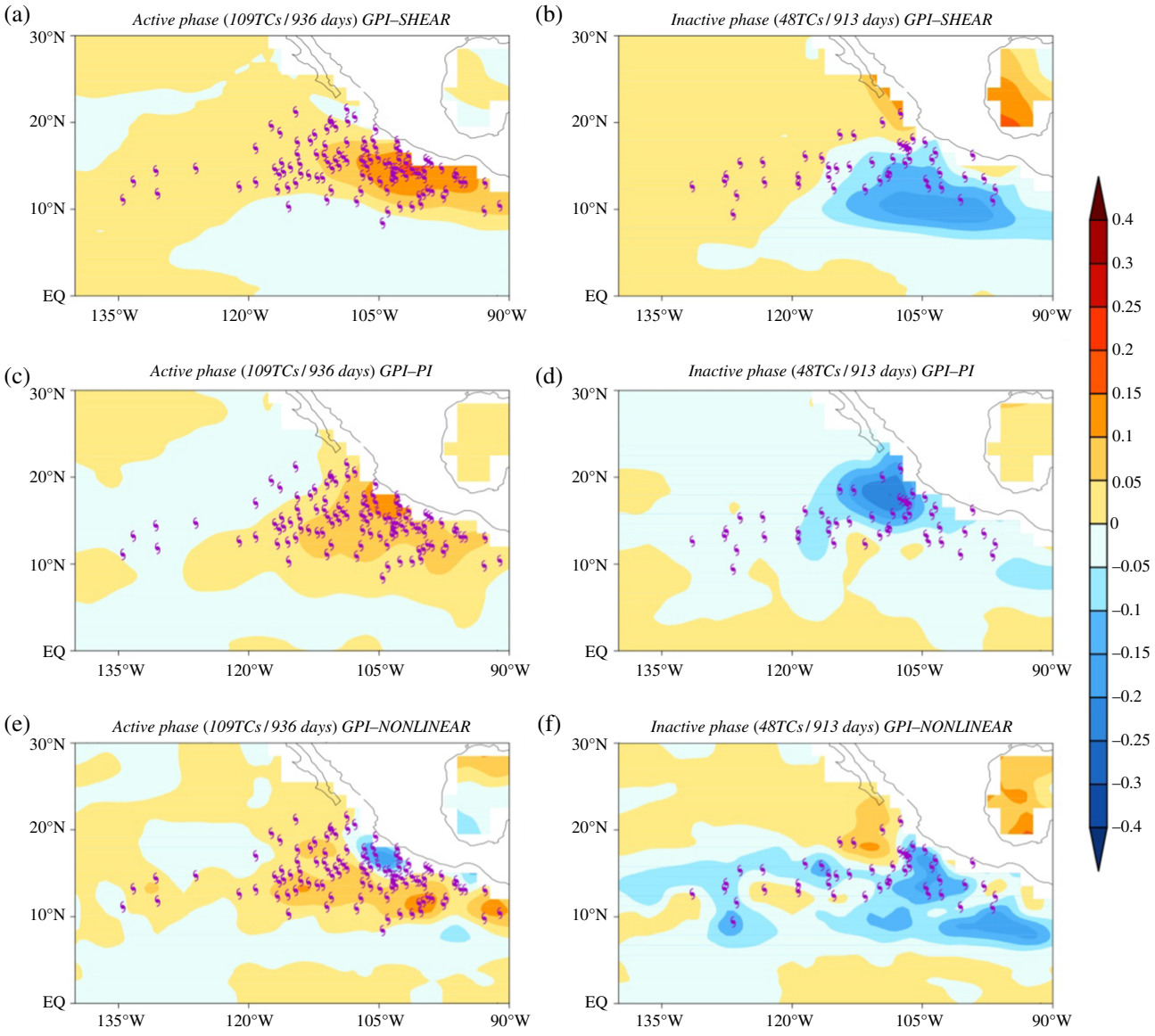

Figure 14. Same as Figure 13 but for: (a) and (b) GPI varying vertical wind shear (GPI-SHEAR); (c) and (d) varying potential intensity (GPI-PI). (e) and (f) are the composite GPI anomalies for the nonlinear term (GPI-NONLINEAR). [Colour figure can be viewed at wileyonlinelibrary.com].

now been studied relatively infrequently. Results from the analysis of 10- to 30-day filtered precipitation suggest that the QBWO strongly modulates ENP TC activity. More TCs are observed during the convectively active phase than during the convectively inactive phase. Furthermore, TCs tend to track more northwestward during the convectively active phase, while TCs tend to track more westward during the convectively inactive phase. These changes in trajectories are related to changes in intensity, with higher ACE and more major hurricanes observed during the convectively active phase and lower ACE and fewer major hurricanes observed during the convectively inactive phase.

The relative importance of the four environmental factors included in the GPI is assessed based upon the analyses of the magnitude and spatial distribution of their anomalies. Mid-level relative humidity and low-level vorticity are found to be the two largest positive contributors to the distribution of GPI anomalies associated with the QBWO. The nonlinear-term is found to be another important factor with vertical wind shear and PI having weaker contributions. Analyses of the magnitude of GPI anomalies suggest that mid-level relative humidity is the most important contributor, with secondary roles from the low-level relative vorticity, vertical wind shear, and PI and a weak contribution from the nonlinear term. Although the results are not identical based upon on the pattern and magnitudes of GPI anomalies, all suggest that mid-level relative humidity and low-level vorticity are the most important modulators of GPI anomalies. These results agree well with results obtained for TC variability at other timescales in previous studies (Camargo *et al.*, 2007, 2009; Jiang *et al.*, 2012). As a final remark, the robustness of the QBWO-TC relationship in this study should be further investigated due to the fact that rainfall associated with TCs may contribute to the QBWO variance.

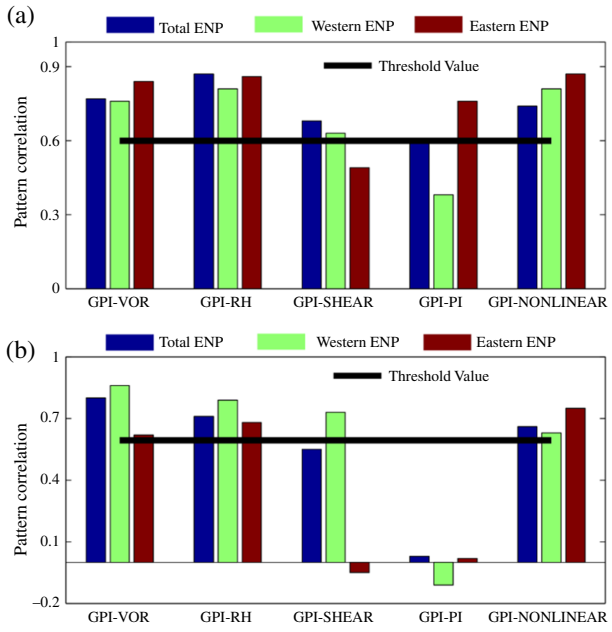

Figure 15. Pattern correlations over the whole ENP basin and eastern and western sub-regions for different QBWO phases, between total GPI anomalies and GPI anomalies with varying 850 hPa vorticity, 600 hPa relative humidity, PI and vertical wind shear and GPI-nonlinear anomalies, respectively. The pattern correlation of 0.6 indicated by a dashed line in (a) and (b) represents a reasonable lower limit for delimiting field forecasts that are synoptically useful, as suggested by Wilks (2006). [Colour figure can be viewed at wileyonlinelibrary.com].

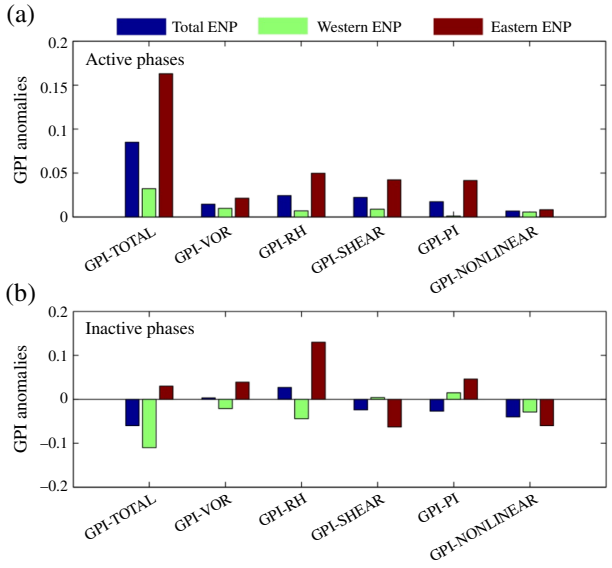

Figure 16. Contribution of the four variables to composite GPI anomalies for: (a) active and (b) inactive QBWO phases over the whole ENP basin and eastern and western sub-regions from May to October for the period 1998–2015. [Colour figure can be viewed at wileyonlinelibrary.com].

Acknowledgements

This research was jointly supported by the National Natural Science Foundation of China (grant nos. 41675072, 41305050 and 41475091), Qing Lan Project (R2017Q01) and the Natural Science Foundation for Higher Education Institutions in Jiangsu Province (12KJA170002, 15KJB170008) and the Priority Academic Program Development of Jiangsu Higher Education Institutions (PAPD).

References

Aiyyer A, Molinari J. 2008. MJO and tropical cyclogenesis in the Gulf of Mexico and eastern Pacific: case study and idealized numerical modeling. *J. Atmos. Sci.* **65**: 2691–2704.

Barrett BS, Leslie LM. 2009. Links between tropical cyclone activity and Madden–Julian oscillation phase in the North Atlantic and Northeast Pacific basins. *Mon. Weather Rev.* **137**: 727–744.

Bell GD, Halpert MS, Schnell RC, Higgins RW, Lawrimore J, Kousky VE, Tinker R, Thiaw W, Chelliah M, Artusa A. 2000. Climate assessment for 1999. *Bull. Am. Meteorol. Soc*. **81**: S1–S50. https://doi.org/10.1175/1520-0477(2000)81[s1:CAF]2.0.CO;2.

Bister M, Emanuel KA. 2002. Low frequency variability of tropical cyclone potential intensity I. Interannual to interdecadal variability. *J. Geophys. Res.* **107**: 4801. https://doi.org/10.1029/2001JD000776.

Camargo SJ, Emanuel KA, Sobel AH. 2007. Use of a genesis potential index to diagnose ENSO effects on tropical cyclone genesis. *J. Clim.* **20**: 4819–4834. https://doi.org/10.1175/JCLI4282.1.

Camargo SJ, Wheeler MC, Sobel AH. 2009. Diagnosis of the MJO modulation of tropical cyclogenesis using an empirical index. *J. Atmos. Sci.* **66**: 3061–3074. https://doi.org/10.1175/2009JAS3101.1.

Cheng CKM, Chan JCL. 2012. Impacts of land use changes and synoptic forcing on the seasonal climate over the Pearl River Delta of China. *Atmos. Environ.* **60**: 25–36.

Chu P-S. 2004. ENSO and tropical cyclone activity. *Hurricanes and Typhoons: Past, Present, and Potential*, Murnane RJ, Liu KB (eds). Columbia University Press: New York, NY, 297–332.

Dee DP, Uppala SM, Simmons AJ, Berrisford P, Poli P, Kobayashi S, Andrae U, Balmaseda MA, Balsamo G, Bauer P, Bechtold P, Beljaars ACM, van de Berg L, Bidlot J, Bormann N, Delsol C, Dragani R, Fuentes M, Geer AJ, Haimberger L, Healy SB, Hersbach H, Hólm EV, Isaksen L, Kållberg P, Köhler M, Matricardi M, McNally AP, Monge-Sanz BM, Morcrette J-J, Park BK, Peubey C, de Rosnay P, Tavolato C, Thépaut JN, Vitart F. 2011. The ERA-interim reanalysis: configuration and performance of the data assimilation system. *Q. J. R. Meteorol. Soc.* **137**(656): 553–597.

Emanuel KA. 2011. Global warming effects on U.S. hurricane damage. *Weather Clim. Soc.* **3**: 261.

Emanuel KA, Nolan DS. 2004. Tropical cyclone activity and the global climate system. Preprints. In *26th Conference on Hurricanes and Tropical Meteorology*, American Meteorological Society, Miami, FL, 10A.2.

Gray WM. 1968. Global view of the origin of tropical disturbances and storms. *Mon. Weather Rev.* **96**: 669–700.

Hall JD, Matthews AJ, Karoly DJ. 2001. The modulation of tropical cyclone activity in the Australian region by the Madden–Julian oscillation. *Mon. Weather Rev.* **129**: 2970–2982.

Huffman GJ, Adler RF, Bolvin DT, Gu G, Nelkin EJ, Bowman KP, Stocker EF, Wolff DB. 2007. The TRMM multi-satellite precipitation analysis: quasi-global, multi-year, combined-sensor precipitation estimates at fine scale. *J. Hydrometeor*. **8**: 33–55.

Jiang X, Waliser DE. 2008. Northward propagation of the subseasonal variability over the eastern Pacific warm pool. *Geophys. Res. Lett.* **35**: L09814. https://doi.org/10.1029/2008GL033723.

Jiang X, Waliser DE. 2009. Two dominant subseasonal variability modes of the eastern Pacific ITCZ. *Geophys. Res. Lett.* **36**: L04704. https://doi.org/10.1029/2008GL036820.

Jiang X, Waliser DE, Li J, Woods C. 2011. Vertical cloud structures of the boreal summer intraseasonal variability based on CloudSat observations and ERA-Interim reanalysis. *Clim Dyn*. **36**: 2219–2332.

Jiang X, Zhao M, Waliser DE. 2012. Modulation of tropical cyclone activity by the tropical intraseasonal oscillation over the Eastern Pacific in a high resolution GCM. *J. Clim.* **25**: 6524–6538.

Jien JY, Gough WA, Bulter K. 2015. The influence of El Nino-Southern Oscillation on tropical cyclone activity in the Eastern North Pacific basin. *J. Clim.* **28**: 2459–2474.

Kim J, Ho C, Kim H, Sui C, Park SK. 2008. Systematic variation of summertime tropical cyclone activity in the western North Pacific in relation to the Madden–Julian oscillation. *J. Clim.* **21**: 1171–1191.

Klotzbach PJ. 2010. On the Madden–Julian oscillation–Atlantic hurricane relationship. *J. Clim.* **23**: 282–293. https://doi.org/10.1175/2009JCLI2978.1.

Landsea CW, Franklin JL. 2013. Atlantic hurricane database uncertainty and presentation of a new database format. *Mon. Weather Rev.* **141**: 3576–3592.

Li CY, Zhou YP. 1995. On quasi-two-week (10-20-day) oscillation in the tropical atmosphere. *Chinese J. Atmos. Sci*. **19**: 435–444 (in Chinese).

Li RCY, Zhou W. 2013. Modulation of western North Pacific tropical cyclone activity by the ISO. Part I: genesis and intensity. *J. Clim.* **26**: 2904–2918.

Madden RA, Julian PR. 1971. Detection of a 40–50 day oscillation in the zonal wind in the tropical Pacific. *J. Atmos. Sci.* **28**: 702–708.

Madden R, Julian P. 1972. Description of global-scale circulation cells in the tropics with a 40–50 day period. *J. Atmos. Sci.* **29**: 1109–1123.

Maloney ED, Dickinson MJ. 2003. The intra-seasonal oscillation and the energetics of summertime tropical western North Pacific synoptic-scale disturbances. *J. Atmos. Sci.* **60**: 2153–2168.

Maloney ED, Hartmann DL. 2000a. Modulation of Eastern North Pacific hurricanes by the Madden–Julian oscillation. *J. Clim.* **13**: 1451–1460. https://doi.org/10.1175/1520-0442(2000)013,1451: MOENPH.2.0.CO;2.

Maloney ED, Hartmann DL. 2000b. Modulation of hurricane activity in the Gulf of Mexico by the Madden–Julian oscillation. *Science* **287**: 2002–2004.

McBride JL, Zehr R. 1981. Observational analyses of tropical cyclone formation: II. comparison of non-developing versus developing systems. *J. Atmos. Sci*. **38**: 1132–1151.

Molinari J, Knight D, Dickinson M, Vollaro D, Skubis S. 1997. Potential vorticity, easterly waves, and eastern Pacific tropical cyclogenesis. *Mon. Weather Rev.* **125**: 2699–2708.

Neena JM, Waliser D, Jiang X. 2017. Model performance metrics and process diagnostics for boreal summer intraseasonal variability. *Clim Dyn*. **48**(5–6): 1661–1683.

North GR, Bell TL, Cahalan RF, Moeng FJ. 1982. Sampling errors in the estimation of empirical orthogonal functions. *Mon. Weather Rev.* **110**: 699–706.

Pielke RA Jr, Landsea CW. 1998. Normalized hurricane damages in the United States, 1925–97. *Weather Forecast.* **13**: 351–361.

Pielke RA Jr, Gratz J, Landsea CW, Collins D, Saunders MA, Musulin R. 2008. Normalized hurricane damage in the United States: 1900–2005. *Nat. Hazards Rev.* **9**: 29–42.

Ralph TU, Gough WA. 2009. The influence of sea-surface temperatures on Eastern North Pacific tropical cyclone activity. *Theor. Appl. Climatol.* **95**: 257–264.

Serra YL, Jiang X, Tian B, Astua J, Maloney ED, Kiladis GN. 2014. Tropical intra-seasonal oscillations and synoptic variability. *Annu. Rev. Environ. Resour.* **39**: 189–215.

Wang R, Wu L, Wang C. 2011. Typhoon track changes associated with global warming. *J. Clim*. **24**: 3748–3752.

Wang C, Wang L, Wang X, Wang D, Wu L. 2016. North-south variations of tropical storm genesis locations in the Western Hemisphere. *Geophys. Res. Lett.* **43**: 11367–11374. https://doi.org/10.1002/2016GL071440.

Weare BC, Nasstrom JS. 1982. Examples of extended empirical orthogonal function analyses. *Mon. Weather Rev.* **110**: 481–485.

Wheeler MC, Hendon HH. 2004. An all-season real-time multivariate MJO index: development of an index for monitoring and prediction. *Mon. Weather Rev.* **132**: 1917–1932.

Wilks DS. 2006. On "field significance" and the false discovery rate. *J. Appl. Meteorol. Clim*. **45**(9): 1181–1189.

Wu L, Wang B. 2004. Assessing impacts of global warming on tropical cyclone tracks. *J. Clim*. **17**: 1686–1698.

Wu L, Wang B, Geng S. 2005. Growing typhoon influence on East Asia. *Geophys. Res. Lett*. **32**: L18703. https://doi.org/10.1029/2005GL022937.

Zhao H, Wu L, Zhou W. 2010. Assessing the influence of ENSO on tropical cyclone prevailing tracks in the western North Pacific. *Adv. Atmos. Sci*. **27**: 1–11.

Zhao H, Chu PS, Hsu PC, Murakami H. 2014. Exploratory analysis of extremely low tropical cyclone activity during the late-season of 2010 and 1998 over the western North Pacific and the South China Sea. *J. Adv. Model. Earth Syst.* **06**(04): 1141–1153.

Zhao H, Jiang X, Wu L. 2015a. Modulation of Northwest Pacific tropical cyclone genesis by the intraseasonal variability. *J. Meteorol. Soc. Jpn* **93**: 1. https://doi.org/10.2151/jmsj.2015-006.

Zhao H, Yoshida R, Raga GB. 2015b. Impact of the Madden–Julian oscillation on western North Pacific tropical cyclogenesis associated with large-scale patterns. *J. Appl. Meteorol. Climatol.* **54**: 1423–1429. https://doi.org/10.1175/JAMC-D-14-0254.1.

Zhao H, Jiang X, Wu L. 2016. Boreal summer synoptic-scale waves over the western North Pacific in multi-model simulations, *J. Clim*. **29**: 4487–4508.

